LLNL-JRNL-2010594

Lawrence Livermore National Laboratory

Direct Functionalization of Established 3D-Printed Aza-Michael Liquid Crystal Elastomers with Donor-Acceptor Stenhouse Adducts Adducts

M Ford

December 2025

ACS Applied Materials and Interfaces

Disclaimer

This work performed under the auspices of the U.S. Department of Energy by Lawrence Livermore National Laboratory under Contract DE-AC52-07NA27344.

Direct Functionalization of Established 3D-Printed Aza-Michael Liquid Crystal Elastomers with Donor-Acceptor Stenhouse Adducts

Sophie Paul,[a†] Jesus Guillen Campos,[b†] Michael J. Ford,[c] Arnab Nandi,[b] Elliot Hawkes,[a] and Javier Read de Alaniz [b]**

S. Paul, E. Hawkes

[a] Department of Mechanical Engineering, University of California, Santa Barbara. Santa Barbara, California 93106, United States.

E-mail: ewhawkes@ucsb.edu

J. Guillen Campos, A. Nandi, J. Read de Alaniz.

[b] Department of Chemistry and Biochemistry, University of California, Santa Barbara. Santa Barbara, California 93106, United States.

E-mail: javier@chem.ucsb.edu

M. J. Ford

[c] Materials Science Division, Lawrence Livermore National Laboratory. Livermore, CA, 94450, United States

Keywords: Donor-Acceptor Stenhouse Adducts, Liquid Crystal Elastomers, Aza-Michael Addition, 3D Printing, Photoactuation

ABSTRACT

Extrusion 3D printing has advanced the manufacturing of complex liquid crystal elastomer (LCE) architectures. In parallel, Donor-Acceptor Stenhouse Adducts (DASAs), a class of white-light-responsive photoswitches, have enabled both photochemical and photothermal LCE actuation. However, DASA-LCEs have yet to be extrusion 3D printed. Two key challenges exist: DASA's inherent sensitivity to heat and radicals can lead to degradation during ink preparation and printing; and small changes in the concentration of the added DASA component impacts the properties of the extrudable ink, requiring re-optimization of well-established 3D printing protocols. To overcome these challenges, we present a post-printing functionalization strategy that circumvents these limitations. Residual secondary amines, inherent to inks synthesized via standard aza-Michael addition, serve as active sites for covalent attachment of DASA photoresponsive groups following printing and crosslinking. Our method means that DASAs can be directly grafted onto 3D printed aza-Michael LCEs without modifying the ink formulation or processing. The resulting DASA-LCEs exhibit wavelength tunability within the visible range and a variety of photothermal and photochemical responses. The post-functionalization can occur within two minutes and enables spatial control of DASA concentration, producing films with tunable color gradients and locally varied photothermal and photochemical responses under visible light. This approach enables the rapid fabrication of DASA-based light-responsive LCEs using established ink formulations, with the potential for the design of complex 3D architectures.

1. INTRODUCTION

Liquid crystal elastomers (LCEs) are appealing materials for applications in soft robotics,[1] biomedical devices,[2] and wearable technologies,[3] due to their unique ability to undergo rapid, reversible shape transformations in response to external stimuli.[4–6] These responses are caused by a reversible nematic to isotropic phase transition, conventionally triggered by heating.[7,8] A long-standing barrier to the widespread adoption of LCEs in soft robotics has been the reliance on complex synthetic protocols and limited scalability, particularly for 3D printed architectures.[8–10] The development of more accessible formulations, such as those obtained from aza-Michael[11] and thiol-Michael addition,[12] has provided more straightforward ways to produce LCEs. Since the application of these chemical strategies to LCEs, Direct-Ink-Write (DIW) printing has been widely used to fabricate centimeter scale soft robots,[13] reducing reliance on more traditional methods of surface or mechanical alignment.[7] Extrusion-based 3D printing enables the fabrication of large-scale three-dimensional structures with nonuniform alignment patterns.[13–18] The degree of alignment and the actuation profile can be precisely controlled by modifying extrusion parameters, such as speed, temperature, and layer height—all of which have been extensively investigated in aza-Michael LCEs.[14,15,17,18] Despite enabling greater tunability and complex shape transformations, conventional LCE systems remain thermally actuated, restricting their operational environments and limiting responsiveness to diverse stimuli.

To address these limitations, light-responsive LCEs have emerged as a powerful alternative, offering remote and spatial-temporal control over the actuation. Two primary strategies have been developed depending on the nature of the light-responsive agent and its compatibility with the LCE matrix. The first approach involves physically incorporating the light-responsive agent into the LCE, which is the least synthetically challenging and relatively straightforward. Carbon nanotubes,[19,20] Ag or Au nanorods[21] and organic dyes[22–26] are common photo-absorbers

incorporated into LCEs, enabling photothermal actuation through localized heating. Photoswitches can also be incorporated this way,[27] but are limited to photothermal actuation. However, with this simplicity of synthesis comes challenges with loading limits and control over dispersion because the light-responsive elements are mixed in and not covalently bound to the LCE monomers[20]. The second approach overcomes these challenges by covalently integrating the element into the polymer network via tailored LCE-based monomer designs. This can be done with organic dyes,[26] but is more common with photoswitches. They can be incorporated along the backbone, as a pendant group, or as crosslinkers, providing a range of actuation behaviors.[28,29] Of these, the most common and robust examples rely on azobenzene,[28–30] but other photoswitches include molecular motors,[31,32] diarylethenes,[33,34] hydrazones,[35] and spiropyrans.[36–38] This approach enables light-induced isomerization of the photoswitches, which in turn drives photochemical and photothermal actuation.[28] These molecules primarily respond to narrowband UV wavelengths, limiting the operational range of photochemically actuated LCEs. Recently, donor-acceptor Stenhouse adducts (DASAs) have been covalently attached to mechanically aligned, siloxane LCEs. They exhibit photochemical and photothermal actuation in response to broadband white light.[36,39] This optical control broadens the range of environments where LCE actuators can operate effectively, overcoming the limitations of thermally and UV-activated systems. Further, DASAs are negative photochromes, making them attractive for use in millimeters-thick LCEs.[39,40] However, DASA-LCEs have yet to be made with DIW 3D printing. To summarize, combining the advantageous properties of DASA-based photochromes with advances in DIW 3D LCE printing provides a path to better soft robots with new actuation capabilities.

Herein, we functionalized 3D printed aza-Michael LCEs with DASAs after printing by leveraging residual secondary amines present in the ink. Our post-functionalization method does

not alter the well-established ink chemistry and does not require the DASA to survive printing. While the first aza-Michael addition is fast and all primary amines are converted to secondary amines in minutes, the subsequent addition is considerably slower and typically incomplete.[41] Despite the known presence of residual secondary amines after oligomerization of LCE formulations, these groups have not yet been utilized to covalently post-functionalize with photochromic molecules. Conveniently, DASA photoswitches require secondary amines to serve as donor group building blocks, presenting a straightforward opportunity for incorporating photochromic functionality via this additive-free post-functionalization strategy, **Figure 1**. With our method, we fabricated a range of DASA-based LCE films with excellent wavelength tunability by varying the acceptor group. Finally, we leveraged the rapid (≈ 2 min) post-functionalization reaction to construct LCE films with spatial control over DASA concentration, leading to multicolored films exhibiting non-uniform light response.

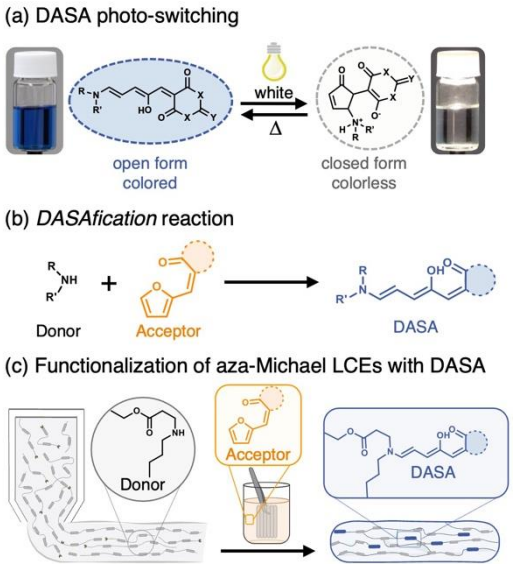

Figure 1. Schematic representation of this study. a) Schematic of DASA photoswitching b) Formation of donor-acceptor Stenhouse adducts by the addition reaction of a secondary amine with an activated furan, termed herein as DASAfication. c) Prescence of a secondary amine in the LCE ink capable of reacting with an activated furan to undergo DASAfication.

2. RESULTS AND DISCUSSION

2.1 Characterization of aza-Michael LC ink

The extensive literature of aza-Michael additions for the polymerization of LCEs suggests a fast and quantitative addition of primary amines to acrylate groups.[41–44 66-68] However, the subsequent reaction of the newly formed secondary amine to a second acrylate group is slower and non-quantitative. Terentjev et. al exploited residual secondary amines to introduce hydrogen-bonding interactions, thereby reinforcing the LCE network.[41] Here, we extend this strategy to covalently post-functionalize aza-Michael 3D-printed LCEs with DASA photoswitches using a well-studied and validated protocol for aza-Michael ink formulation. Specifically, we adopted the ink formulation reported by Lewis, et. al, which yields optically transparent films using a 1.1:1.0 molar ratio of RM257 and C6BAPE mesogens and *n*-butylamine as a chain extender.[18] Butylated hydroxytoluene (BHT) was added to suppress radical formation during the oligomerization, and 2,2-dimethoxy-2-phenhylacetophenone (DMPA) was introduced as the photoinitiator, shown in **Figure 2a**. Detailed formulation can be found in the experimental section.

The key design feature of this post-functionalization method lies in the deliberate use of the incomplete aza-Michael addition, which preserves reactive amines in the as-printed LCE. These amines serve as handles for subsequent reaction with activated furan to generate DASA photoswitches directly within the polymer network. To quantify the concentration of secondary amines present under these conditions, the stepwise aza-Michael reaction between butylamine and

the mesogenic acrylates RM257 and C6BAPE was monitored using ^{1}H NMR spectroscopy. As shown in **Figure 2b** and **Figure 2c**, the transformation proceeds through two distinct stages: rapid conversion of the primary amine to the secondary intermediate, followed by a slower second addition forming the tertiary amine. Full kinetic analysis, including quantification of the acrylate conversion, is provided in Supplementary Information Figure S1-S4. Within ten minutes, the primary amine is fully consumed, and the concentration of secondary amine reaches a peak before gradually decreasing over five hours. Concurrently, the rate of tertiary amine formation is highest within the first 2.5 hours and slows down through the 5-hour mark. Under these conditions, approximately 10 mol% of secondary amines remain in the ink formulation, serving as the functional handle for DASA formation after oligomerization, printing, and crosslinking (**Figure 2d**). Extending the ink curing time has little effect on this concentration.

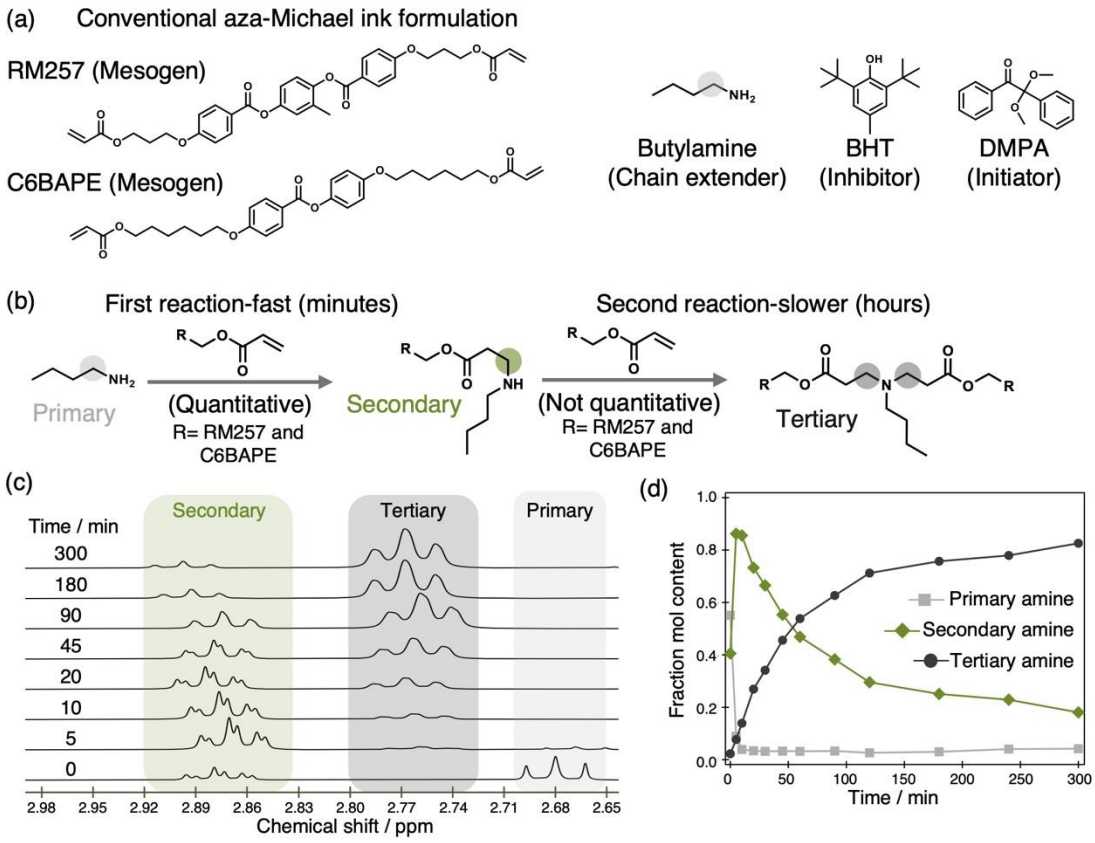

Figure 2. a) Ink formulation previously reported in the literature. b) First and second addition reaction between primary and secondary amine and acrylate functional groups. c) 1H NMR traces showing the region where primary amine converts to secondary and tertiary amine. d) Fraction of primary, secondary and tertiary amine present as a function of time.

For photoresponsive extrusion-based LCEs, the properties that govern actuation (order parameter, T_{NI}, optical transparency, etc.) depend heavily on the shear profile during extrusion, which is influenced by viscosity.[45] The viscosity is controlled primarily by oligomerization time, as is the evolution of functional groups discussed previously. To understand this connection, the oligomer viscosity was measured as a function of reaction time. The optimal viscosity occurred around four hours into the oligomerization. This oligomerization time was used for all LCEs prepared. At this time, the secondary amine content and the viscosity remain relatively stable in response to small differences in time, which is key for reproducibility and consistent

DASAfication of the subsequent films. After this time, the ink became too viscous to be extruded using our experimental setup, affecting the alignment and the optical properties of the films, Figure S5. Such increase in viscosity can be coupled to the increase in the degree of polymerization in these timeframes. To determine the degree of oligomerization of the ink, the molecular weight of the ink was followed by gel permeation chromatography as a function of reaction time. Figure S6-S7 shows that after five hours, the molecular weight of the ink reaches only 5.0 kg/mol. In summary, while the viscosity of the ink evolves over time and can affect printability, a significant fraction of reactive secondary amines persists within these timeframes. The amount of residual amine directly dictates the extent of subsequent DASA post-functionalization, underscoring its importance for ensuring reproducibility across aza-Michael LCE methodologies (Figure S8).

2.2 Functionalization of aza-Michael LCE films using DASA

2.2.1 Rapid DASAfication of aza-Michael LCEs.

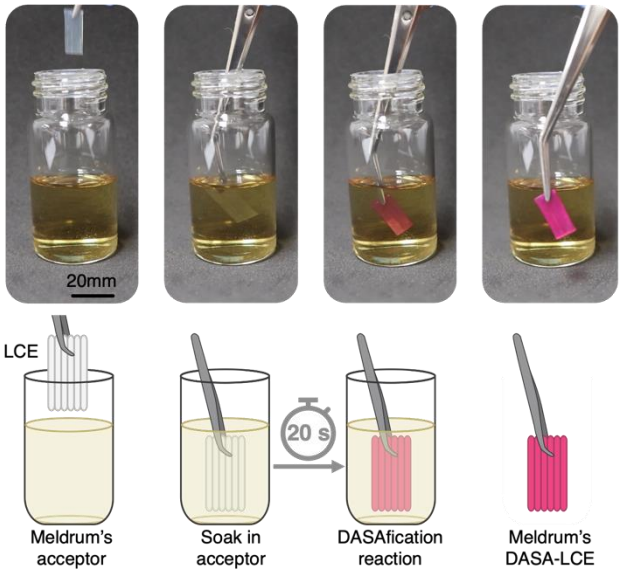

Figure 3. Fast functionalization of aza-Michael LCEs (film dimensions 10 mm × 20 mm × 0.3 mm) with Meldrum's acid activated furan.

The overall degree of functionalization is governed by several variables, including the initial concentration of secondary amines in the printed network, diffusion of the DASA acceptor, and the intrinsic efficiency of the DASA-forming reaction. Precise quantification of these factors in a cross-linked elastomer matrix is challenging; however, time-dependent absorption UV-vis absorption spectroscopy was used to monitor DASA formation with Meldrum's acid, barbituric acid, CF_3-oxazolone, and CF_3-pyrazolone acceptors using the oligomer ink employed for 3D printing. As expected, the reaction rate depends strongly on the acceptor identity: CF_3-pyrazolone and CF_3-oxazolone reached maximum absorbance within ≈ 20 min (indicative of full conversion), while barbituric acid showed only partial conversion after 40 min (Figure S9). In these studies, the acceptor concentration was held constant at 10 mg mL^{-1}; nonetheless, faster and more quantitative conversion can be achieved by increasing acceptor concentration or extending reaction times (Figures S10). Diffusion of the acceptor into the network also plays a critical role, particularly for thicker films. For example, functionalization of 1.2 mm-thick 3D-printed LCE films in acetone solution of Meldrum's acid (1.07 g / 10 mL) revealed a distinct shell structure upon bisection, with a functionalized layer extending≈ 500 μm after 20 min (Figure S11and S12).

Guided by these control experiments, aza-Michael LCE films were 3D printed with dimensions of 10 mm × 20 mm × 0.3 mm and directly subjected to post-functionalization. As shown in Figure 3 and Video S1, an as-printed LCE was immersed in a 10 wt.% solution of Meldrum's acid derived acceptor in acetone for 20 seconds. A distinct pink coloration rapidly developed within the LCE, contrasting sharply with the yellow solution, indicating the successful formation of the DASA photoswitch via reaction with residual secondary amines. Because functionalization proceeds through chemical reaction between the secondary amines and activated furan, issues such as clumping, poor dispersion and leaching are largely irrelevant. Moreover, this

post-functionalization strategy is compatible with a range of DASA-based acceptors and the rate of covalent reactions is correlated to the electrophilicity of the activated furan. For example, when an oxazolone-derived acceptor, featuring enhanced electrophilicity, was employed, the reaction proceeded to completion in just one second, as shown in Figure S13 and Video S2. This high speed further underscores the efficiency of the covalent functionalization pathway.

2.2.2 Spectral tunability of Aza-Michael DASA LCEs. Aza-Michael DASA LCEs were prepared with six different acceptors to demonstrate color tunability and to illustrate the generality of the process, **Figure 4a**. Meldrum acid derivative (Mel), Barbituric acid derivative (Bar), CF_3-Oxazolone (Oxa), CF_3-Pyrazolone (Pyr_{CF_3}), CH_3-Pyrazolone (Pyr_{CH_3}) and OMe-Pyrazolone (Pyr_{OMe}) were selected as the acceptor groups due to their different properties, **Figure 4b**. The as-printed LCEs were soaked in 100 mg in 10 mL acetone acceptor solution. The Meldrum acid, Barbituric acid, CH_3-Pyrazolone, OMe-Pyrazolone were soaked for one minute and CF_3-Pyrazolone and CF_3-Oxazolone were soaked for 10 sec. Solid-state-UV-Visible spectroscopy was used to determine the absorbance bands of the 3D-printed LCE films, shown in **Figure 4c**. By changing only the acceptor solution, 3D-printed LCEs with tunable colors and absorbance

wavelengths can be fabricated in minutes. This tunability is essential for deployment as orthogonal and selective light-responsive soft actuators.

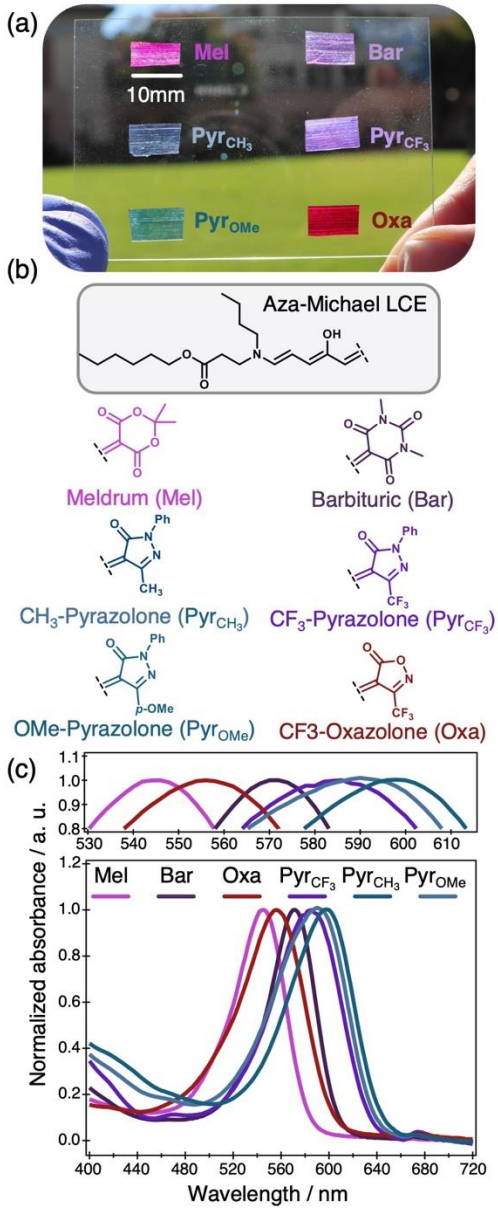

Figure 4. a) Picture of 3D Printed DASA-LCEs. b) Chemical structures of the DASAs present in the functionalized LCEs. c) Absorbance profile of the absorption bands of the DASA LCEs in the solid-state.

2.2.3 Electronic properties of DASAs inside the LCE polymer matrix. DASA's photoswitching behavior is influenced by the electronic properties of the acceptor groups, which can be measured using solvachromatic slopes. Solvatochromic slope is defined as the change of the absorbance

maxima as a function of solvent polarity. A more neutral form of DASA will have a low solvatochromic slope and a more zwitterionic/charged DASA will have a higher slope. Low solvatochromic slopes have been correlated with better photoswitching in a range of solvents and polymer matrices.[46–48] Conversely, DASAs exhibiting high solvatochromic slopes show minimal or no photoswitching under the same conditions. As such, DASAs can function as either a photoswitch or photothermal agent depending on the ground state structure and environment.

To estimate the electronic and solvatochromic properties of the DASAs synthesized in the crosslinked LCE polymer matrix, which can be hard to characterize by conventional techniques such as ^{1}H NMR and UV-Vis spectroscopy, a small-molecule DASA model system was synthesized. In this model system, hexyl 3-(butylamino)propanoate served as the donor/secondary amine. This donor was chosen because of its similar electronic properties to the amine in the ink formulation. Analyzing their absorbance profiles of the small molecule DASA adduct in different solvents, Figure S14-S21, yields a wide range of solvatochromic slopes as seen in **Figure 5a**. From these slopes, one can predict if DASA will behave predominantly as a photothermal agent or negative photoswitch. To illustrate how these small molecule solvatochromic studies correlate with the differences in the DASA light-response observed within the 3D printed LCEs, we analyze the photoresponse of two orthogonal DASA LCEs. Films with OMe-Pyrazolone (slope = -24 nm) and CF_3-Pyrazolone (slope = -90 nm) were exposed to 300 mW/cm^2 of broadband white light. As expected, the OMe-Pyrazolone film switched to the colorless closed form, whereas the CF_3-Pyrazolone film remained highly colored, generating a stronger photothermal effect and molecular contraction (**Figure 5b** and Video S3-S4). Both contraction and color change are reversible upon removal of the light source with no photofatigue observed after 15 cycles or after extended irradiation exposure (Figure S22 and S23). Photothermal contraction of the CF_3-Pyrazolone LCE

film was confirmed using infrared imaging. Upon exposure to white light (300 mW/cm^2), the CF_3-Pyrazolone film rapidly heated above T_{NI}, in contrast to the unfunctionalized control, which remained below the transition temperature. This difference supports the photothermal origin of actuation **(**Video S5**).**

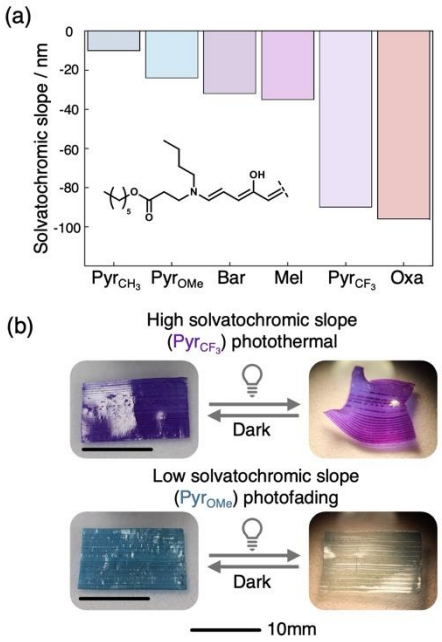

Figure 5. a) Solvatochromic slopes of the DASAs present in the LCEs showing a wide variety of solvatochromic slopes. B) Distinct actuation behavior of the DASA LCEs with low and high solvatochromic values.

2.3 DASA Patterning Capabilities

The rapid kinetics of the DASAfication reaction enable precise spatial control over photoswitch distribution within LCE films. Depending on the acceptor used, functionalization is complete within seconds to minutes. This fast reaction window allows for partial submersion of films in organic solvents without concerns of solvent evaporation, uncontrolled diffusion, or swelling-induced strain—factors that typically hinder patterning fidelity in systems requiring

prolonged exposure. As shown in **Figure 6a**, the intensity of color can be varied over the course of a few seconds. In the same manner, a color gradient can be formed in a single film by slowly pulling the film out of the acceptor solution as shown in **Figure 6b**.

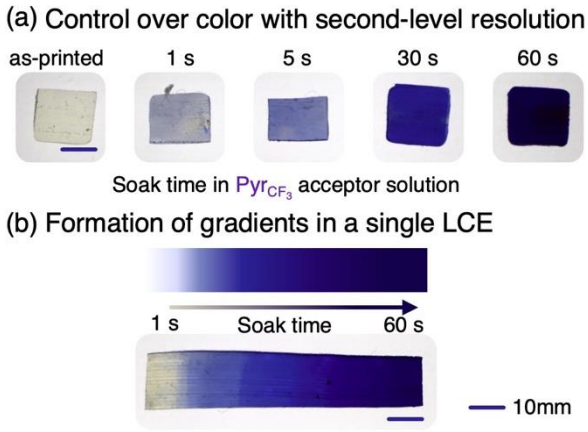

Figure 6. a) aza-Michael LCEs functionalized with CF_3-Pyrazolone showing the increasing loading as a function of soaking times. b) Formation of gradients of color in a single film using CF_3-Pyrazolone acceptor. Scale bar = 10mm.

To further demonstrate the patterning capabilities enabled by DASA functionalization in the 3D-printed elastomers, a shell-like functionalization was carried out on the surface of the films Figure S24-S25. A 6 mm x 15 mm x 5 mm LCE was submerged in an aqueous solution of 10 mg of Meldrum's acid acceptor in 10 mL of water. Water was chosen as the solvent for the reaction because it does not swell into the polymer matrix, constraining the reaction to a surface level. Successful functionalization of the LCE was observed after four hours of reaction. To demonstrate the interfacial reaction, the film was cut through its cross-sectional area, Figure S26, showing functionalization of the outer 20 μm of the LCE surface while the rest of the film remained uncolored. This approach provides a convenient route to selectively functionalize the surface of the LCEs, which is not possible with physical blending.

Traditionally, producing non-uniform responses in an LCE requires spatial modification of the alignment, $T_{NI,}$ crosslink density or composition, before polymerization.[30,49,50] Alternatively, we can rapidly program regions of varying DASA concentration within the same LCE film just by dipping. This results in nonuniform actuation profiles that depend on the DASA functionalization patterns and can be programmed after polymerization, contrasting from conventional techniques. In the same manner, multicolored DASA LCEs can be fabricated by exposing different regions to different acceptor solutions, which exhibit distinct actuation behaviors, as discussed previously. To demonstrate this, two identical and uniformly aligned rectangles (same formulation, same batch of ink, same printing conditions) were fabricated with the long axis parallel to the nematic director. Then, we patterned the rectangles to get two actuation behaviors that stem from the same starting LCE. The first one is constituted by a concentration gradient using CH_3-Pyrazolone as the acceptor solution. The resulting gradient DASA-LCE contracts asymmetrically under a symmetric white light stimulus, **Figure 7a** and Video S6. To visualize the asymmetric contraction, a white box showcases the higher magnitude of contraction only in the region where the LCE contains more DASA molecules.

Similarly, a horizontal stripe pattern using two distinct DASAs was fabricated by dipping the film halfway into one acceptor solution (CH_3-Pyrazolone), then dipping the other half in a different

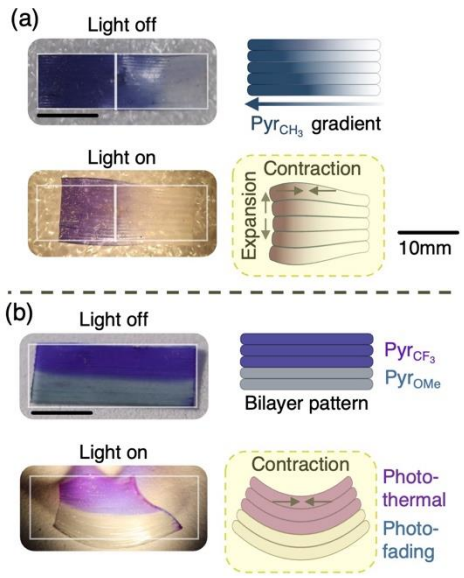

Figure 7. a) Gradient of DASA functionalization enabling asymmetric contraction of a 3D printed film with white light. The film is pinned at its center, represented by the vertical white line to illustrate the contraction gradient between the areas of high and low DASA loading. B) Contraction of a bilayer pattern of two DASAs with different solvatochromic behavior.

solution (Pyr_{OMe}). When the entire LCE is exposed to white light, the asymmetric contraction always occurs towards the side containing the better photothermal DASA regardless of the direction of light irradiation, shown in **Figure 7b** and Video S7. This user-friendly approach to the functionalization of 3D printed LCEs might enable novel ways to selectively actuate more complex structures in future studies.

3. CONCLUSIONS

DASAs were covalently incorporated into an unmodified aza-Michael LCE formulation by leveraging residual secondary amines as both an active handle and precursor photoswitch formation. The LCE, as printed, was swelled in a solution which reacted with these secondary amines to produce DASA after polymerization. The functionalized LCEs exhibit tunable wavelength absorption, colors, DASA concentration, and actuation behavior. Furthermore, the functionalization reaction occurs within two minutes, enabling the formation of single-color

gradients and multi-color patterns, producing asymmetric actuation. The tunable properties of the DASA-LCEs demonstrated in this work can be used in the design, fabrication, and implementation of light-responsive soft robotics in future research.

4. EXPERIMENTAL SECTIONS

4.1 Synthesis of LC ink. The LC ink was synthesized using a previously reported aza-Michael chain extension.[18] A 1:1 molar ratio of the mesogens, 2.29 g of 4-(6-(acryloyloxy)hexyloxy)-phenyl 4-(6-(acryloyloxy)hexyloxy)benzoate and 2.5 g of 1,4-bis[4-(3-acryloyloxypropyloxy)benzoyloxy]-2-methylbenzene, along with 0.2 wt.% butylated hydroxytoluene and 2 wt% Irgacure 651 was combined and heating to 100 °C. Then, this mixture was mixed in a centrifugal mixer (FlackTek) and allowed to cool for 2 minutes until the solution was below 70 °C. Then, 0.56 g *n*-butylamine was added to the mixture such that the molar ratio of mesogen acrylates to amine is 1.1:1. Note, cooling the solution is important because the boiling point of *n*-butylamine is 85 °C. This solution was mixed in the centrifugal mixer again for 1 min before reacting for 4 hours in an oven at 85 °C under ambient atmosphere. The ink was cooled to room temperature and stored in the dark overnight prior to use. The ink was then transferred to a syringe for 3D printing.

4.2 3D Printing LCEs. The LCEs were 3D printed using a HYREL3D Engine SR with KR2-15 extruders. Samples of various sizes were 3D printed using 0.3 mm nozzles at 30 °C, with a print speed of 5 mm/s and a layer height of 150 μm. During the printing process, the LCEs were cross linked with 200 mW/cm^2 365 nm UV flashlights and post-cured in a curing chamber for 2 hours. To prevent inconsistencies, the short edges of the rectangles were cut off, where the extruder changes direction.

4.3 Synthesis of DASA small molecules. The following general experimental procedure was used for the synthesis of the DASA-small molecules used to determine the solvatochromic slopes of the DASAs present in the LCEs. Hexyl 3-(butylamino)propanoate (300 mg, 1.3 mmol, 1 equivalent) was added to a one-dram vial and dissolved in 1 mL of dichloromethane. To this solution, 2 mmol (1.5 equivalents) of the activated furan acceptor was added. The reactions were stirred overnight, except for the oxazolone solution which was stirred for only 10 minutes. After this, the reactions were purified by flushing them with dichloromethane through a small plug of silica gel to elute the starting materials. Then, the silica plug was flushed with a mixture of 10 % methanol in dichloromethane to elute the DASA target compound. The solution was concentrated under reduced pressure to yield the DASA products. Detailed reaction yields and spectral information can be found in the supplementary information.

4.4 General method for LCE DASAfication.

As printed LCEs were soaked in 10 mg/mL acetone acceptor solution for a given specified time. Then the film was removed from the acceptor solution and rinsed with acetone. Upon which the film was soaked in acetone for 10 minutes to remove excess acceptor. This was repeated until no color was observed in the acetone solution.

ASSOCIATED CONTENT

Supporting Information.

The following files are available free of charge.

Supplementary Information- Materials, Methods, Detailed synthesis and characterization of compounds (PDF)

Supplementary Videos 1-6 (MP4)

Video S1- Functionalization of LCE with Meldrums

Video S2- Functionalization of LCE with Oxazolone

Video S3- White light-induced photofading of OMe Pyrazalone LCE

Video S4- White light-induced photothermal contraction of CF3 Pyrazalone LCE

Video S5- Infrared imaging video of photothermal contraction of CF3 Pyrazolone LCE

Video S6- Nonuniform actuation of LCE with DASA gradient

Video S7-Directional actuation of LCE with 2 acceptors

AUTHOR INFORMATION

Corresponding Author

*Javier Read de Alaniz, email: javier@chem.ucsb.edu

*Elliot Hawkes, email: ewhawkes@ucsb.edu

Author Contributions

The manuscript was written through contributions of all authors. All authors have given approval to the final version of the manuscript. ‡These authors contributed equally.

ACKNOWLEDGMENT

This work was supported by the BioPACIFIC Materials Innovation Platform of the National Science foundation under Award No. DMR-1933487 and CMMI-1944816. SP gratefully acknowledges financial support from the National Science Foundation Graduate Research Fellowship (Grant No. 2139319). Part of this work was performed under the auspices of the U.S. Department of Energy by Lawrence Livermore National Laboratory under Contract DE-AC52-07NA27344, LLNL-JRNL-2010594.

REFERENCES

(1) Yu, Y.; Ikeda, T. Soft Actuators Based on Liquid-Crystalline Elastomers. *Angew. Chem. Int. Ed.* **2006**, *45* (33), 5416–5418. https://doi.org/10.1002/anie.200601760.

(2) Shaha, R. K.; Merkel, D. R.; Anderson, M. P.; Devereaux, E. J.; Patel, R. R.; Torbati, A. H.; Willett, N.; Yakacki, C. M.; Frick, C. P. Biocompatible Liquid-Crystal Elastomers Mimic the Intervertebral Disc. *J. Mech. Behav. Biomed. Mater.* **2020**, *107*, 103757. https://doi.org/10.1016/j.jmbbm.2020.103757.

(3) Forman, J.; Kilic Afsar, O.; Nicita, S.; Lin, R. H.-J.; Yang, L.; Hofmann, M.; Kothakonda, A.; Gordon, Z.; Honnet, C.; Dorsey, K.; Gershenfeld, N.; Ishii, H. FibeRobo: Fabricating 4D Fiber Interfaces by Continuous Drawing of Temperature Tunable Liquid Crystal Elastomers. In *Proceedings of the 36th Annual ACM Symposium on User Interface Software and Technology*; ACM: New York, NY, USA, 2023; pp 1–17. https://doi.org/10.1145/3586183.3606732.

(4) Zeng, H.; Wasylczyk, P.; Wiersma, D. S.; Priimagi, A. Light Robots: Bridging the Gap between Microrobotics and Photomechanics in Soft Materials. *Adv. Mater.* **2018**, *30* (24). https://doi.org/10.1002/adma.201703554.

(5) Bisoyi, H. K.; Urbas, A. M.; Li, Q. Soft Materials Driven by Photothermal Effect and Their Applications. *Adv. Opt. Mater.* **2018**, *6* (15). https://doi.org/10.1002/adom.201800458.

(6) Herbert, K. M.; Fowler, H. E.; McCracken, J. M.; Schlafmann, K. R.; Koch, J. A.; White, T. J. Synthesis and Alignment of Liquid Crystalline Elastomers. *Nat. Rev. Mater.* **2022**, *7* (1), 23–38. https://doi.org/10.1038/s41578-021-00359-z.

(7) Finkelmann, H.; Kock, H.; Rehage, G. Investigations on Liquid Crystalline Polysiloxanes 3. Liquid Crystalline Elastomers — a New Type of Liquid Crystalline Material. *Makromol. Chem. Rapid Commun.* **1981**, *2* (4), 317–322. https://doi.org/10.1002/marc.1981.030020413.

(8) Schätzle, J.; Kaufhold, W.; Finkelmann, H. Nematic Elastomers: The Influence of External Mechanical Stress on the Liquid-crystalline Phase Behavior. *Makromol. Chem.* **1989**, *190* (12), 3269–3284. https://doi.org/10.1002/macp.1989.021901224.

(9) Küpfer, J.; Finkelmann, H. Nematic Liquid Single Crystal Elastomers. *Makromol. Chem. Rapid Commun.* **1991**, *12* (12), 717–726. https://doi.org/10.1002/marc.1991.030121211.

(10) Noël, C.; Navard, P. Liquid Crystal Polymers. *Prog. Polym. Sci.* **1991**, *16* (1), 55–110. https://doi.org/10.1016/0079-6700(91)90007-8.

(11) Ware, T. H.; McConney, M. E.; Wie, J. J.; Tondiglia, V. P.; White, T. J. Voxelated Liquid Crystal Elastomers. *Science* **2015**, *347* (6225), 982–984. https://doi.org/10.1126/science.1261019.

(12) Yakacki, C. M.; Saed, M.; Nair, D. P.; Gong, T.; Reed, S. M.; Bowman, C. N. Tailorable and Programmable Liquid-Crystalline Elastomers Using a Two-Stage Thiol–Acrylate Reaction. *RSC Adv.* **2015**, *5* (25), 18997–19001. https://doi.org/10.1039/C5RA01039J.

(13) Kotikian, A.; McMahan, C.; Davidson, E. C.; Muhammad, J. M.; Weeks, R. D.; Daraio, C.; Lewis, J. A. Untethered Soft Robotic Matter with Passive Control of Shape Morphing and Propulsion. *Sci. Robot.* **2019**, *4* (33). https://doi.org/10.1126/scirobotics.aax7044.

(14) Kotikian, A.; Truby, R. L.; Boley, J. W.; White, T. J.; Lewis, J. A. 3D Printing of Liquid Crystal Elastomeric Actuators with Spatially Programed Nematic Order. *Adv. Mater.* **2018**, *30* (10). https://doi.org/10.1002/adma.201706164.

(15) Ren, L.; Li, B.; He, Y.; Song, Z.; Zhou, X.; Liu, Q.; Ren, L. Programming Shape-Morphing Behavior of Liquid Crystal Elastomers via Parameter-Encoded 4D Printing. *ACS Appl. Mater. Interfaces* **2020**, *12* (13), 15562–15572. https://doi.org/10.1021/acsami.0c00027.
(16) Ambulo, C. P.; Burroughs, J. J.; Boothby, J. M.; Kim, H.; Shankar, M. R.; Ware, T. H. Four-Dimensional Printing of Liquid Crystal Elastomers. *ACS Appl. Mater. Interfaces* **2017**, *9* (42), 37332–37339. https://doi.org/10.1021/acsami.7b11851.
(17) Wang, Z.; Wang, Z.; Zheng, Y.; He, Q.; Wang, Y.; Cai, S. Three-Dimensional Printing of Functionally Graded Liquid Crystal Elastomer. *Sci. Adv.* **2020**, *6* (39). https://doi.org/10.1126/sciadv.abc0034.
(18) Kotikian, A.; Watkins, A. A.; Bordiga, G.; Spielberg, A.; Davidson, Z. S.; Bertoldi, K.; Lewis, J. A. Liquid Crystal Elastomer Lattices with Thermally Programmable Deformation via Multi-Material 3D Printing. *Adv. Mater.* **2024**, *36* (34), 2310743. https://doi.org/10.1002/ADMA.202310743.
(19) Ji, Y.; Marshall, J. E.; Terentjev, E. M. Nanoparticle-Liquid Crystalline Elastomer Composites. *Polymers* **2012**, *4* (1), 316–340. https://doi.org/10.3390/polym4010316.
(20) Skillin, N. P.; Bauman, G. E.; Kirkpatrick, B. E.; McCracken, J. M.; Park, K.; Vaia, R. A.; Anseth, K. S.; White, T. J. Photothermal Actuation of Thick 3D-Printed Liquid Crystalline Elastomer Nanocomposites. *Adv. Mater.* **2024**, *36* (34). https://doi.org/10.1002/adma.202313745.
(21) Wang, Y.; Liu, J.; Yang, S. Multi-Functional Liquid Crystal Elastomer Composites. *Appl. Phys. Rev.* **2022**, *9* (1). https://doi.org/10.1063/5.0075471.
(22) Marshall, J. E.; Terentjev, E. M. Photo-Sensitivity of Dye-Doped Liquid Crystal Elastomers. *Soft Matter* **2013**, *9* (35), 8547. https://doi.org/10.1039/c3sm51091c.
(23) Wani, O. M.; Zeng, H.; Priimagi, A. A Light-Driven Artificial Flytrap. *Nat. Commun. 2017 81* **2017**, *8* (1), 1–7. https://doi.org/10.1038/ncomms15546.
(24) Deng, Z.; Li, K.; Priimagi, A.; Zeng, H. Light-Steerable Locomotion Using Zero-Elastic-Energy Modes. *Nat. Mater. 2024 2312* **2024**, *23* (12), 1728–1735. https://doi.org/10.1038/s41563-024-02026-4.
(25) Camacho-Lopez, M.; Finkelmann, H.; Palffy-Muhoray, P.; Shelley, M. Fast Liquid-Crystal Elastomer Swims into the Dark. *Nat. Mater.* **2004**, *3* (5), 307–310. https://doi.org/10.1038/nmat1118.
(26) Shahsavan, H.; Aghakhani, A.; Zeng, H.; Guo, Y.; Davidson, Z. S.; Priimagi, A.; Sitti, M. Bioinspired Underwater Locomotion of Light-Driven Liquid Crystal Gels. *Proc. Natl. Acad. Sci.* **2020**, *117* (10), 5125–5133. https://doi.org/10.1073/pnas.1917952117.
(27) Hsu, L. Y.; Mainik, P.; Münchinger, A.; Lindenthal, S.; Spratte, T.; Welle, A.; Zaumseil, J.; Selhuber-Unkel, C.; Wegener, M.; Blasco, E. A Facile Approach for 4D Microprinting of Multi-Photoresponsive Actuators. *Adv. Mater. Technol.* **2023**, *8* (1), 2200801. https://doi.org/10.1002/ADMT.202200801.
(28) Garcia-Amorós, J.; Finkelmann, H.; Velasco, D. Influence of the Photo-Active Azo Cross-Linker Spacer on the Opto-Mechanics of Polysiloxane Elastomer Actuators. *J Mater Chem* **2011**, *21* (4), 1094–1101. https://doi.org/10.1039/C0JM02502J.
(29) Pang, X.; Lv, J.; Zhu, C.; Qin, L.; Yu, Y. Photodeformable Azobenzene-Containing Liquid Crystal Polymers and Soft Actuators. *Adv. Mater.* **2019**, *31* (52), 1904224. https://doi.org/10.1002/adma.201904224.
(30) Ahn, S. K.; Ware, T. H.; Lee, K. M.; Tondiglia, V. P.; White, T. J. Photoinduced Topographical Feature Development in Blueprinted Azobenzene-Functionalized Liquid

Crystalline Elastomers. *Adv. Funct. Mater.* **2016**, *26* (32), 5819–5826. https://doi.org/10.1002/adfm.201601090.
(31) Hou, J.; Long, G.; Zhao, W.; Zhou, G.; Liu, D.; Broer, D. J.; Feringa, B. L.; Chen, J. Phototriggered Complex Motion by Programmable Construction of Light-Driven Molecular Motors in Liquid Crystal Networks. *J. Am. Chem. Soc.* **2022**, *144* (15), 6851–6860. https://doi.org/10.1021/jacs.2c01060.
(32) Long, G.; Deng, Y.; Zhao, W.; Zhou, G.; Broer, D. J.; Feringa, B. L.; Chen, J. Photoresponsive Biomimetic Functions by Light-Driven Molecular Motors in Three Dimensionally Printed Liquid Crystal Elastomers. *J. Am. Chem. Soc.* **2024**, *146* (20), 13894–13902. https://doi.org/10.1021/jacs.4c01642.
(33) Lahikainen, M.; Kuntze, K.; Zeng, H.; Helantera, S.; Hecht, S.; Priimagi, A. Tunable Photomechanics in Diarylethene-Driven Liquid Crystal Network Actuators. *ACS Appl. Mater. Interfaces* **2020**, *12* (42), 47939–47947. https://doi.org/10.1021/acsami.0c12735.
(34) Hebner, T. S.; Podgórski, M.; Mavila, S.; White, T. J.; Bowman, C. N. Shape Permanence in Diarylethene-Functionalized Liquid-Crystal Elastomers Facilitated by Thiol-Anhydride Dynamic Chemistry. *Angew. Chem. Int. Ed.* **2022**, *61* (11). https://doi.org/10.1002/anie.202116522.
(35) Ryabchun, A.; Li, Q.; Lancia, F.; Aprahamian, I.; Katsonis, N. Shape-Persistent Actuators from Hydrazone Photoswitches. *J. Am. Chem. Soc.* **2019**, *141* (3), 1196–1200. https://doi.org/10.1021/jacs.8b11558.
(36) Guillen Campos, J.; Park, M.; Wu, Y.; Sandlass, S.; Novikov, E. M.; Bailey, S. J.; Gordon, M.; Timofeeva, T. V.; Read de Alaniz, J. Synthesis of Photoresponsive Liquid Crystal Elastomers: A General Chemical Approach. *J. Mater. Chem. A* **2025**, *13* (21), 15773–15781. https://doi.org/10.1039/D5TA01043H.
(37) Zuo, B.; Wang, M.; Lin, B.-P.; Yang, H. Photomodulated Tricolor-Changing Artificial Flowers. *Chem. Mater.* **2018**, *30* (21), 8079–8088. https://doi.org/10.1021/acs.chemmater.8b04204.
(38) Han, D.; Wang, X.; Liu, S.; Zhang, Y.; Li, C.; Gao, Y.; Zhang, J. Mechanochromic Response of Spiropyran-Incorporated Liquid Crystalline Elastomer Network and the Mechanochromic Enhancement by Nano Zinc Oxide. *Adv. Mater. Technol.* **2023**, *8* (17), 2300175. https://doi.org/10.1002/admt.202300175.
(39) Guillen Campos, J.; Tobin, C.; Sandlass, S.; Park, M.; Wu, Y.; Gordon, M.; Read de Alaniz, J. Photoactivation of Millimeters Thick Liquid Crystal Elastomers with Broadband Visible Light Using Donor–Acceptor Stenhouse Adducts. *Adv. Mater.* **2024**, *36* (35). https://doi.org/10.1002/ADMA.202404932.
(40) Helmy, S.; Leibfarth, F. A.; Oh, S.; Poelma, J. E.; Hawker, C. J.; Read de Alaniz, J. Photoswitching Using Visible Light: A New Class of Organic Photochromic Molecules. *J. Am. Chem. Soc.* **2014**, *136* (23), 8169–8172. https://doi.org/10.1021/ja503016b.
(41) Zou, W.; Lin, X.; Terentjev, E. M.; Zou, W.; Lin, X.; Terentjev, E. M. Amine-Acrylate Liquid Single Crystal Elastomers Reinforced by Hydrogen Bonding. *Adv. Mater.* **2021**, *33* (30), 2101955. https://doi.org/10.1002/ADMA.202101955.
(42) González, G.; Fernández-Francos, X.; Serra, À.; Sangermano, M.; Ramis, X. Environmentally-Friendly Processing of Thermosets by Two-Stage Sequential Aza-Michael Addition and Free-Radical Polymerization of Amine–Acrylate Mixtures. *Polym. Chem.* **2015**, *6* (39), 6987–6997. https://doi.org/10.1039/c5py00906e.

(43) Retailleau, M.; Pierrel, J.; Ibrahim, A.; Croutxé-Barghorn, C.; Allonas, X. Sequenced Click Chemistry and Photopolymerization: A New Approach toward Semi-interpenetrating Polymer Networks. *Polym. Adv. Technol.* **2017**, *28* (4), 491–495. https://doi.org/10.1002/pat.3914.
(44) Genest, A.; Portinha, D.; Fleury, E.; Ganachaud, F. The Aza-Michael Reaction as an Alternative Strategy to Generate Advanced Silicon-Based (Macro)Molecules and Materials. *Prog. Polym. Sci.* **2017**, *72*, 61–110. https://doi.org/10.1016/j.progpolymsci.2017.02.002.
(45) Ford, M. J.; Telles, R.; Porcincula, D. H.; Reyes, C. G.; Paul, S.; Hendrix, I.; Hawkes, E.; Read de Alaniz, J.; Cook, C. C.; Lee, E. Versatile Liquid Crystal Elastomer Formulations Using Amine-Acrylate Chemistry and Processing for Advanced Manufacturing. *ACS Appl. Eng. Mater.* **2025**, *3* (5), 1389–1398. https://doi.org/10.1021/acsaenm.5c00176.
(46) Clerc, M.; Tekin, C.; Ulrich, S.; Freire, R. V. M.; Salentinig, S.; Bruns, N.; Boesel, L. F. Donor–Acceptor Stenhouse Adduct-Polydimethylsiloxane-Conjugates for Enhanced Photoswitching in Bulk Polymers. *Macromol. Rapid Commun.* **2022**, *43* (15). https://doi.org/10.1002/marc.202200120.
(47) Stricker, F.; Peterson, J.; Sandlass, S. K.; de Tagyos, A.; Sroda, M.; Seshadri, S.; Gordon, M. J.; Read de Alaniz, J. Selective Control of Donor-Acceptor Stenhouse Adduct Populations with Non-Selective Stimuli. *Chem* **2023**, *9* (7), 1994–2005. https://doi.org/10.1016/j.chempr.2023.05.011.
(48) Peterson, J. A.; Neris, N. M.; Read De Alaniz, J. Tethered Together: DASA Design towards Aqueous Compatibility. *Chem. Sci.* **2023**, *14* (45), 13025–13030. https://doi.org/10.1039/D3SC02835F.
(49) Ware, T. H.; Perry, Z. P.; Middleton, C. M.; Iacono, S. T.; White, T. J. Programmable Liquid Crystal Elastomers Prepared by Thiol–Ene Photopolymerization. *ACS Macro Lett.* **2015**, *4* (9), 942–946. https://doi.org/10.1021/acsmacrolett.5b00511.
(50) Yang, R.; Zhao, Y. Non-Uniform Optical Inscription of Actuation Domains in a Liquid Crystal Polymer of Uniaxial Orientation: An Approach to Complex and Programmable Shape Changes. *Angew. Chem.* **2017**, *129* (45), 14390–14394. https://doi.org/10.1002/ange.201709528.

TOC

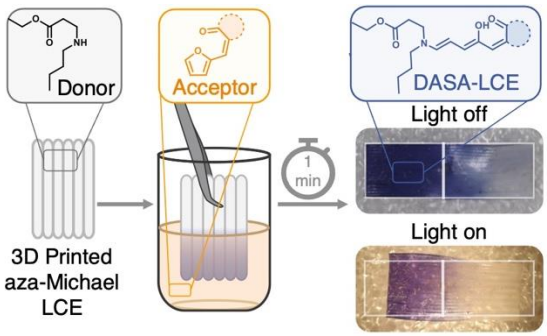
Donor
Acceptor
DASA-LCE
Light off
1
min
Light on
3D Printed
aza-Michael
LCE